A Moment Ratio RFI Detection Algorithm That Can Detect Pulsed Sinusoids of Any Duty Cycle

Roger D. De Roo, *Member, IEEE*, and Sidharth Misra

***Abstract*—The kurtosis statistic is an effective detector of pulsed sinusoidal radio frequency interference (RFI) in a microwave radiometer, but it fails to detect RFI when the pulsed sinusoid is present for exactly half of the integration period. That is, the kurtosis is blind at an RFI duty cycle of 50%. In this letter, we explore the possibilities of using a higher order statistic to eliminate this detection blind spot in the kurtosis statistic and to improve RFI detection performance. The sixth-order statistic does have sensitivity at an RFI duty cycle of 50%, but sensitivity is relatively low. In addition, it has a sensitivity comparable with the kurtosis for short duty cycle RFI, under certain circumstances.**

***Index Terms*—Detectors, digital radio, interference suppression, microwave radiometry.**

I. Introduction

RADIO frequency interference (RFI) is a problem in microwave radiometry [1]–[3]. The kurtosis statistic has been demonstrated to be an effective detector of pulsed sinusoidal RFI in a microwave radiometer [4]–[6]. The kurtosis is the fourth central moment m_4 of the predetected voltage normalized by the square of the second central moment, m_2. The second central moment is the variance of the voltage and is proportional to the radiometer system temperature. In the absence of interference, the thermal processes give rise to a Gaussian distribution of the voltage, for which the kurtosis is equal to three. The kurtosis can greatly exceed three, when short pulses of RFI are present, and is less than three when relatively strong continuous-wave RFI is present. However, the kurtosis is also three when pulsed-sinusoidal interference is present for exactly 50% of the radiometer integration period, regardless of the interference strength. Thus, the kurtosis statistic is blind to the interference when it is present with a 50% duty cycle.

Several techniques exist for overcoming the weaknesses of the kurtosis. For example, cross-frequency comparisons are very useful for detecting 100% duty cycle sinusoids (e.g., [7]). We are also investigating the possibility of combining accumulations from different integration periods to create longer synthetic integration periods, for which the duty cycle of any RFI present will likely be altered and potentially more easily detected [8]. In [9], we explored the effectiveness of using the voltage's sixth moment to supplement the kurtosis in order to eliminate the kurtosis blind spot. In this letter, we extend those sixth-moment results to form a single detection statistic for which there is no blind spot.

Manuscript received September 30, 2009; revised January 6, 2010. Date of publication March 22, 2010; date of current version April 29, 2010.

The authors are with the Department of Atmospheric, Oceanic, and Space Sciences, University of Michigan, Ann Arbor, MI 48109-2143 USA (e-mail: deroo@umich.edu).

Color versions of one or more of the figures in this paper are available online at http://ieeexplore.ieee.org.

Digital Object Identifier 10.1109/LGRS.2010.2043051

II. Kurtosis Detection Algorithm

In a digital radiometer, the variance, σ^2 of the Gaussian-distributed intermediate frequency (IF) voltage at the analog-to-digital converter (ADC) is proportional to the radiometer system temperature T_{SYS}

$$\frac{\sigma^2}{Z_0} = kT_{SYS}BG \tag{1}$$

where Z_0 is the matching impedance of the digitizer, k is the Boltzmann's constant, B is the radiometer bandwidth, and G is the radiometer analog gain. This variance can be estimated by calculating the first and second moments of the digitized voltage. This is performed as follows: The firmware accumulates the sum of the first $(n = 1)$ and second $(n = 2)$ powers of the digitized voltages x_i

$$S_n = \sum_{i=1}^{N_s} x_i^n \tag{2}$$

where N_s is a predetermined number of samples to be summed in each integration period. Typically, the accumulations S_n are offloaded from the radiometer for postprocessing. The nth moment about the origin μ_n of the output of the ADC is determined from $\mu_n = S_n/N_s$. From these, the second central moment m_2 is found: $m_2 = \mu_2 - \mu_1^2$; and neglecting digitization effects, the variance is estimated as $m_2 v_0^2$, where v_0 is the voltage span of one bin of the ADC. The average of the digitized voltage μ_1 is collected because the center of the zero bin usually does not correspond to the IF ground.

In the absence of RFI, all central moments higher than m_2 are known because the geophysical signal of interest is Gaussian noise. In this instance, the odd central moments are zero, and the even central moments are given by

$$m_{2n} = (2n-1)\cdot(2n-3)\cdots 3\cdot 1\cdot \sigma^{2n}. \tag{3}$$

Thus, all of the moment ratios are well known in the absence of RFI. For example, the kurtosis, given by $R = m_4/m_2^2$, is expected to be three.

The most common form of RFI, at least at L-band, is from radars [10], and this RFI can be modeled as a pulsed sinusoid of amplitude A (at the ADC input) and duty cycle d. The duty cycle is the proportion of time that the sinusoid is present in a given integration period. For example, radar pulses typically have a short duty cycle, while broadcast carriers have duty cycles of 100%. Frequency and phase modulation are

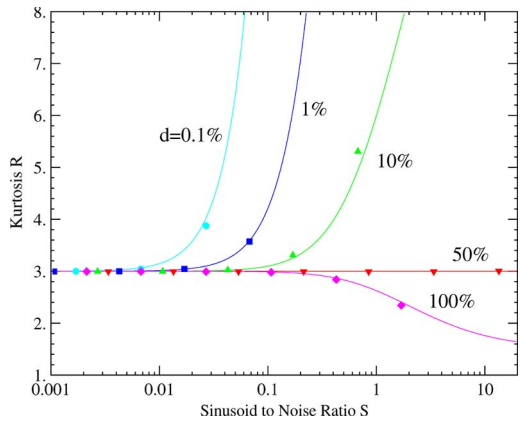

Fig. 1. (Marks) Measured and (curves) modeled kurtosis as a function of RFI strength for five duty cycles. The lack of deflection of the statistic at 50% duty cycle indicates that this statistic is blind to this RFI.

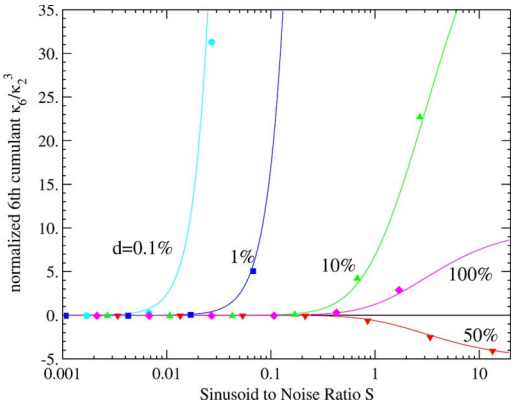

Fig. 2. (Marks) Measured and (curves) modeled normalized sixth cumulant as a function of RFI strength for five duty cycles. A deflection of the statistic at 50% duty cycle indicates that this statistic, unlike the kurtosis, can detect such RFI. However, there are blind spots on both sides of the 50% duty cycle.

expected to be well described by the voltage distribution of this model [11].

The kurtosis R is an excellent detector of the presence of impulsive RFI [5]. The third and fourth powers of the voltage are accumulated in addition to the first and second. From these, we find the fourth central moment via [12]

$$m_4 = \mu_4 - 4\mu_3\mu_1 + 6\mu_2\mu_1^2 - 3\mu_1^4. \tag{4}$$

The expected value of R is given by [5]

$$E(R) = 3\left(1 + \left(\frac{1}{2d} - 1\right)\left(1 + \frac{1}{S}\right)^{-2}\right) \tag{5}$$

where $S = dA^2/2\sigma^2$ is the average power ratio of RFI to radiobrightness. In the absence of RFI, i.e., $S = 0$, $E(R) = 3$. Any significant deflection of R from three is an indicator of the presence of RFI. However, $d = 50\%$ is another condition for which $E(R) = 3$. Thus, the kurtosis statistic has a blind spot at 50% duty cycle pulsed sinusoidal RFI. This blindness can be seen in Fig. 1, where even the strong RFI at 50% duty cycle is indistinguishable from negligibly small RFI at the left edge of the figure. In addition, the RFI must be quite strong for duty cycles between 20% and 100% for detection by the kurtosis. The data for this figure was collected in a benchtop laboratory experiment for which details are described in [6].

III. Higher Order Statistics

To overcome this blind spot in the kurtosis, we investigate the possibility of using statistics of order that is higher than four to identify RFI at 50% duty cycle. Additional resources must be devoted in the radiometer to accumulate higher order powers of the voltage according to (2). The central moments are calculated from the accumulations in a similar fashion to m_4 described earlier. An arbitrary even moment of the pulsed sinusoidal voltage distribution is derived in the Appendix and is given by

$$\frac{m_{2n}}{\sigma^{2n}} = \frac{(2n)!}{2^n n!}\left[(1+S)^n + \sum_{k=1}^{n}\left(\frac{1}{k!d^{k-1}} - 1\right)\frac{n!S^k}{k!(n-k)!}\right]. \tag{6}$$

Since the binomial term cancels out in every moment-ratio test, the leading term with dependence on the duty cycle is proportional to S^2. However, its dependence has the same form as the kurtosis dependence on the duty cycle: At 50%, the coefficient of S^2 is zero. Thus, while the sensitivity of the higher order moments is not zero at the 50% duty cycle, the RFI must be relatively strong to significantly change the value of these moments from their RFI-free values.

The cumulants turn out to be easier to analyze than that of the moments because, as is shown in the Appendix, the $2n$th cumulant is proportional to S^n. However, the variation of an estimate of a moment calculated from a finite number of voltage samples grows with the moment order [12]. The same is true for the cumulants. This growth of the sample variance coupled with the high-order dependence of the cumulant on the RFI means that the higher order statistics are progressively less sensitive to low-power RFI.

IV. Sixth-Order Statistics

The lowest order test with no blindness at the 50% duty cycle is a sixth moment ratio, and the relevant cumulants, given in terms of the central moments, are [12]

$$\kappa_2 = m_2 \tag{7}$$

$$\kappa_4 = m_4 - 3m_2^2 \tag{8}$$

$$\kappa_6 = m_6 - 15m_4m_2 - 10m_3^2 + 30m_2^3. \tag{9}$$

The normalized fourth cumulant $R_4 = \kappa_4/\kappa_2^2$ is exactly the same as the kurtosis but with a constant value of three subtracted from it. The expected value of the normalized sixth cumulant $R_6 = \kappa_6/\kappa_2^3$ is given by

$$E(R_6) = \frac{5}{2}\left(\frac{1}{d^2} - 9\frac{1}{d} + 12\right)\left(1 + \frac{1}{S}\right)^{-3}. \tag{10}$$

In the absence of RFI (i.e., $S = 0$), $R_6 = 0$. A comparison of this expression with the same laboratory data is shown in Fig. 2.

To identify any blind spots in R_6, we solve for d

$$d = \frac{2}{9 \pm \sqrt{33 + \frac{8}{5}R_6(1 + 1/S)^3}}. \tag{11}$$

Thus, $d = 2/(9 \pm \sqrt{33})$ are the duty cycles at which $R_6 = 0$ and are indistinguishable from the RFI-free situation. These duty cycles correspond to $d = 13.56\%$ and $d = 61.44\%$. Thus, R_6 has two blind spots, but at least, they are not at the same location as the one blind spot of the kurtosis.

V. Variance of the Detection Statistics

Geary [13] has shown that for the RFI-free case, the sample variance is independent from all of the higher orders of the normalized sample moments. This result indicates that both the kurtosis and the normalized sixth cumulant are unbiased detectors of RFI: The statistics of the second moment will not be altered by using these detectors to reject values of the second moment as corrupted by RFI.

In the Appendix, we have applied the methods of [12] for calculating the standard error of a statistic, and we find that, in the absence of RFI

$$\sigma_4^2 = \frac{24}{N} \tag{12}$$

$$\sigma_6^2 = \frac{720}{N} \tag{13}$$

where σ_n^2 is the sample variance of the nth cumulant ratio and N is the number of independent samples. The variance of the sixth-order statistic is much higher than that of the kurtosis.

The false-alarm rate (FAR) for RFI detection using one of these statistics is determined by setting how many standard deviations z away from the RFI-free expectation the statistic must be to flag RFI. Provided the number of independent samples N is sufficiently large that the statistic can be assumed to be Gaussian, the FAR is given by $FAR = 1 - \mathrm{erf}(z/\sqrt{2})$. Following [5], we shall arbitrarily set the probability of detection of RFI to $1 - FAR$ for the purpose of defining a minimum detectable RFI $S_{\min}$. For a constant FAR (CFAR) and thus a fixed z, the minimum detectable RFI as a function of N, S, and d is

$$\left(E(R_n) \pm z\sigma_n\right)|_{S=0} = \left(E(R_n) \mp z\sigma_n\right)|_{S=S_{\min}}. \tag{14}$$

An analysis of the standard error of the cumulant ratio with RFI, given in the Appendix, confirms that the use of the RFI-free value for σ_n is appropriate on both sides of this equation. Since, from (5) and (10), $E(R_4) = E(R_6) = 0$ for the RFI-free case $(S = 0)$

$$\pm 2z\sqrt{\frac{24}{N}} = 3\left(\frac{1}{2d} - 1\right)(1 + 1/S_{\min})^{-2} \tag{15}$$

$$\pm 2z\sqrt{\frac{720}{N}} = \frac{5}{2}\left(\frac{1}{d^2} - 9\frac{1}{d} + 12\right)(1 + 1/S_{\min})^{-3}. \tag{16}$$

For illustration, Fig. 3 shows the contours of this minimum detectable RFI $S_{\min}$ for R_4 and R_6 with $N = 100$ kilosamples and $z = 1$ (chosen arbitrarily), corresponding to a FAR of 33%. The sensitivity of the kurtosis is generally better than that of the normalized sixth cumulant since the RFI power S that triggers an RFI detection is lower except near the kurtosis' 50% duty cycle blind spot.

While the system engineer has two parameters N and z with which to set the performance of the RFI detection system, these two parameters do not have independent effects on the detectability of the RFI. That is, the parameter that determines the performance of a moment-ratio test is the number of standard errors of the moment-ratio statistic. This single parameter is proportional to $z/\sqrt{N}$.

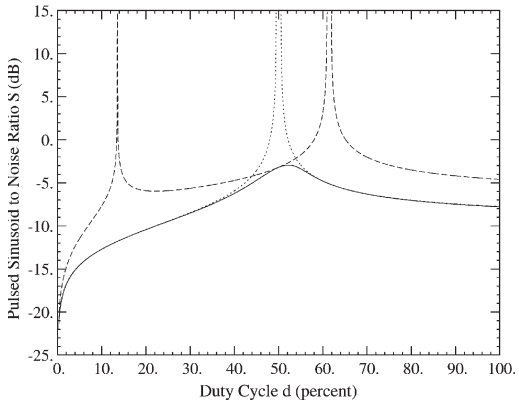

Fig. 3. Minimum detectable pulsed sinusoid to noise ratio using the (dotted) kurtosis and (dashed) normalized sixth cumulant with equal FAR. The solid line shows the performance of a combination of the two tests.

If more than the mere presence of RFI is desired, such as a determination of the nature of persistent interferers, the combination of the fourth and sixth cumulant tests yield information not available to the kurtosis test. For example, in the event that RFI is detected, the use of both the fourth and sixth cumulants permits a rough approximation of the duty cycle of the interferer. This is because $E(R_4) < 0$ for $d > 50\%$, and $E(R_6) < 0$ for $13.6\% < d < 61.4\%$.

Since the two cumulant ratios are independent in the absence of RFI, they can be combined to produce an RFI detection test statistic R_c^2 which does not have a blind spot with respect to the duty cycle, i.e.,

$$R_c^2 = \left(\frac{R_4}{\sigma_4}\right)^2 + \left(\frac{R_6}{\sigma_6}\right)^2. \tag{17}$$

This test statistic R_c^2 can be considered to be exponentially distributed with unit variance in the absence of RFI. Fig. 3 shows how this test statistic provides a significant improvement over the kurtosis near duty cycles of 50%.

VI. Performance of the Detection Statistics

By equating the values of $(1 + 1/S_{\min})$ in the CFAR equations, we can identify those RFI powers at which the detectability using kurtosis and the normalized sixth cumulant are equal. This leaves us with one equation in N/z^2 and d, the solution of which is shown as the solid curve in Fig. 4. This contour locates the number of samples as a function of duty cycle where the kurtosis is equally sensitive as the normalized sixth cumulant. Above the curve, the kurtosis is more sensitive to RFI. At large N, the kurtosis is the best option except at the 50% duty cycle. Below the curve, the normalized sixth cumulant appears to be more sensitive, with this statistic never superior to the kurtosis at the blind spots of 13% and 61% duty cycle.

This curve of equal sensitivity is derived using an assumption that the distribution of the normalized fourth and sixth moments is normal, which it is not true except if the number of samples becomes very large. As shown in the Appendix, the skew of the normalized sixth moment is greater than the skew of the

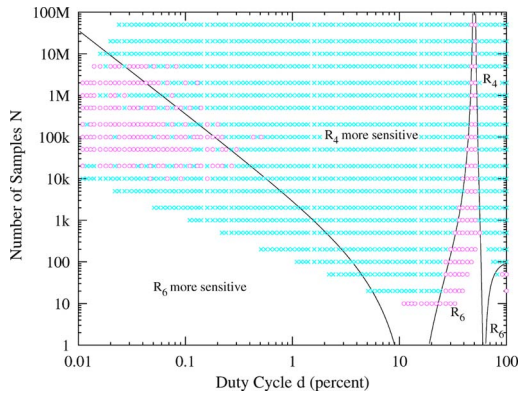

Fig. 4. Comparison of the sensitivity of the normalized fourth and sixth cumulants. The solid curve divides the regions of superior sensitivity of the kurtosis and the normalized sixth moment to pulsed sinusoidal RFI, according to (15) and (16) when $z = 1$. The circles denote a Monte Carlo simulation where the normalized sixth moment is more sensitive than the kurtosis, and crosses denote where the kurtosis is superior to the normalized sixth moment. The indistinct border between the two marks for $N > 10$ kilosamples and $d < 0.3\%$ indicates comparable performance of the two tests.

kurtosis. The normalized sixth cumulant requires 37 times the number of samples as the kurtosis for the same skewness of the distribution when no RFI is present.

To explore the consequences of the nonnormality of the distributions of the normalized sixth and fourth cumulants on the relative sensitivity of these tests to pulsed sinusoidal RFI, a series of Monte Carlo simulations were performed. The mean and standard deviation of the two tests were calculated, both with and without RFI, and the separation of the means in terms of the number of standard deviations was calculated. The test with the greatest separation between the with- and without-RFI conditions was deemed more sensitive. The results of these Monte Carlo simulations are superimposed on Fig. 4. The normalized sixth moment is clearly more sensitive than the kurtosis near $d = 50\%$ but is also sometimes more sensitive than the kurtosis when $N > 10$ kilosamples and $d < 0.3\%$. An inspection of the separations between the RFI and RFI-free simulations shows that the two tests are comparable in this region of the figure. For fewer number of samples, the distribution of the normalized sixth moment is so far from normal that the kurtosis is unambiguously more sensitive to RFI, except near the kurtosis blind spot of $d \approx 50\%$.

VII. Conclusion

When the RFI in a radiometer is due to a pulsed sinusoid with a duty cycle of 50%, the kurtosis produces a result which is indistinguishable from an observation that is free of RFI, regardless of the strength of the RFI. While higher order central moments do not have this kind of blind spot at a 50% duty cycle, the leading terms of the expansion of these normalized even central moments in terms of the RFI to system temperature ratio S are proportional to $(1/2d - 1)$. Thus, higher order moments do eliminate the blind spot in the kurtosis, but their sensitivity to RFI is less than that of the kurtosis at most other duty cycles. The normalized sixth cumulant, for example, has two blind spots: at $d = 13\%$ and at $d = 61\%$. However, the sensitivity of the normalized sixth moment is comparable with the kurtosis for short duty-cycle pulsed RFI when $N > 10$ kilosamples.

A combination of the normalized fourth and sixth cumulants yields a test statistic that has sensitivity to pulsed sinusoidal RFI at all duty cycles of the pulses.

Considering the additional resources needed within a receiver to collect m_6, the marginal RFI detection performance improvements due to the sixth-order statistics appear to make these statistics unworthy of being included in radiometers for most geophysical applications. In some specialized circumstances, such as covert emitter detection, this technique may prove useful since additional information regarding the duty cycle is available when compared with a detector using only the kurtosis.

Appendix
Statistical Properties of a Noisy Pulsed Sinusoid

The probability density function (pdf) of the voltage of Gaussian noise with a pulsed sinusoid is the convolution of a zero-mean σ^2-variance Gaussian pdf $p_g(v)$ and of a pulsed sinusoid pdf $p_{ps}(v)$ as given by [5, eq. (12)], i.e.,

$$p(v) = p_g(v) \otimes p_{ps}(v) \tag{18}$$

$$p_g(v) = \frac{1}{\sqrt{2\pi}\sigma} e^{-v^2/2\sigma^2} \tag{19}$$

$$p_{ps}(v) = (1-d)\delta(v) + \frac{d}{\pi\sqrt{A^2 - v^2}} \tag{20}$$

where v is the voltage, A is the amplitude of the pulsed sinusoid, d is the pulsed-sinusoid duty cycle $(0 < d \leq 1)$, $\delta(v)$ is the Dirac delta function, and $\otimes$ denotes convolution.

Since both $p_g(v)$ and $p_{ps}(v)$ are even functions of v, $p(v)$ is also an even function of v, and the odd moments and odd cumulants of the pulsed sinusoidal density function are zero.

The characteristic function is the Fourier transform of the pdf. Thus, the characteristic function of the noisy pulsed sinusoid is the product of the characteristic functions of the noise and pulsed sinusoids

$$\phi(x) = \int_{-\infty}^{\infty} e^{jxv} p(v) dv = \phi_g(x)\phi_{ps}(x) \tag{21}$$

$$= e^{-\sigma^2 x^2/2} \left[1 + d\left(J_0(Ax) - 1\right)\right]. \tag{22}$$

The characteristic function of the pulsed sinusoid, employing a Bessel function, is evaluated with [14, eq. 8.411 (10)].

If the characteristic function can be expanded in a Maclaurin series, the moments of the distribution are the coefficients [12]

$$\phi(x) = \sum_{r=0}^{\infty} m_r \frac{(jx)^r}{r!} \tag{23}$$

where m_r is the rth moment of $p(v)$, $r!$ denotes the factorial of r, and j is the imaginary constant.

Expanding the exponential and the Bessel functions as Maclaurin series and combining the two series with [14, eq. (0316)], we obtain

$$\frac{m_{2n}}{\sigma^{2n}} = \frac{(2n)!}{2^n n!}\left[1 + d\sum_{k=1}^{n}\frac{n!}{(k!)^2(n-k)!}\left(\frac{S}{d}\right)^k\right] \tag{24}$$

where $S = dA^2/2\sigma^2$ is the pulsed sinusoid to noise power ratio.

This expression agrees with the results of the second through eighth moments given by [14, eq. (15–18)] and is expressed in a slightly different form in (6).

The cumulants are the coefficients of the Maclaurin series of the natural logarithm of the characteristic function

$$\ln\phi(x) = \sum_{r=1}^{\infty}\kappa_r\frac{(jx)^r}{r!} \tag{25}$$

$$= \sigma^2\frac{(jx)^2}{2!} + \sum_{n=1}^{\infty}(2n)!c_n\left(\frac{A}{2}\right)^{2n}\frac{(jx)^{2n}}{(2n)!}$$

$$c_n = d\left(\frac{1}{(n!)^2} - \frac{1}{n}\sum_{k=1}^{n-1}\frac{k}{\left((n-k)!\right)^2}c_k\right) \tag{26}$$

where the series expansion of the natural logarithm of the Bessel function is performed with [15, eq. (6.364)]. The cumulants κ_{2r} are proportional to A^{2r} and thus, also proportional to S^r. As a result, the higher order cumulants are less sensitive to low-power RFI than lower order cumulants.

The standard error of the cumulant ratios is derived by expanding the cumulants in terms of central moments and using the techniques of [12, Ch. 10]. The standard error of the normalized fourth cumulant is the same as that of the kurtosis and is given by [5, eq. (21)], and is reproduced here for reference

$$\sigma_4^2 = \frac{1}{Nm_2^6}\left[m_8m_2^2 - 4m_6m_4m_2 + 4m_4^3 - m_4^2m_2^2\right]. \tag{27}$$

The standard error of the normalized sixth cumulant is

$$\sigma_6^2 = \frac{1}{Nm_2^8}\Big[m_{12}m_2^2 - 30m_{10}m_2^3 - 6m_8m_6m_2 + 60m_8m_4m_2^2 + 225m_8m_2^4 + 9m_6^2m_4 + 86m_6^2m_2^2 - 180m_6m_4^2m_2 - 840m_6m_4m_2^3 + 900m_4^3m_2^2 - 225m_4^2m_2^4\Big]. \tag{28}$$

When the cumulant is even, the distribution of a normalized cumulant ratio approaches Gaussian, as the number of independent samples increases. In the absence of RFI, the second and third moment of the $2p$th sample cumulants are ([12, Ch. 12])

$$E\left((\hat{\kappa}_{2p})^2\right) = (2p)!\frac{\kappa_2^{2p}}{N} + O(N^{-2}) \tag{29}$$

$$E\left((\hat{\kappa}_{2p})^3\right) = \left(\frac{(2p)!}{p!}\right)^3\frac{\kappa_2^{3p}}{N^2} + O(N^{-3}). \tag{30}$$

From this, the skewness is readily calculated

$$\text{skew}(R_{2p}) = \frac{E\left((\hat{\kappa}_{2p})^3\right)}{\left(E\left((\hat{\kappa}_{2p})^2\right)\right)^{3/2}} = \left(\frac{\sqrt{(2p)!}}{p!}\right)^3\frac{1}{\sqrt{N}} + O(N^{-1}). \tag{31}$$

Thus, for a given integration period and value of N, the skewness of the RFI-free normalized sixth cumulant is 6.085 larger than the skewness of the RFI-free normalized fourth cumulant. In terms of the number of samples needed to achieve a particular skewness of the test statistic in the RFI-free case, the sixth normalized cumulant requires 37 times the number of samples as does the normalized fourth cumulant. For example, in [5], we suggested that the kurtosis can be safely considered as normally distributed if the number of samples exceeds 50 kilosamples. For a similarly small skewness in the normalized sixth cumulant, the number of samples should exceed 1.85 megasamples.

REFERENCES

[1] E. G. Njoku, P. Ashcroft, T. K. Chan, and L. Li, "Global survey and statistics of radio-frequency interference in AMSR-E land observations," *IEEE Trans. Geosci. Remote Sens.*, vol. 43, no. 5, pp. 938–947, May 2005.

[2] D. M. Le Vine and M. Haken, "RFI at L-band in synthetic aperture radiometers," in *Proc. IEEE IGARSS*, Toulouse, France, Jul. 21–25, 2003, vol. 3, pp. 1742–1744.

[3] S. W. Ellingson and J. T. Johnson, "A polarimetric survey of radio-frequency interference in C- and X-bands in the continental United States using WindSat radiometry," *IEEE Trans. Geosci. Remote Sens.*, vol. 44, no. 3, pp. 540–548, Mar. 2006.

[4] C. S. Ruf, S. Gross, and S. Misra, "RFI detection and mitigation for microwave radiometry with an agile digital detector," *IEEE Trans. Geosci. Remote Sens.*, vol. 44, no. 3, pp. 694–706, Mar. 2006.

[5] R. D. De Roo, S. Misra, and C. S. Ruf, "Sensitivity of the kurtosis statistic as a detector of pulsed sinusoidal RFI," *IEEE Trans. Geosci. Remote Sens.*, vol. 45, no. 7, pp. 1938–1946, Jul. 2007.

[6] R. D. De Roo and S. Misra, "A demonstration of the effects of digitization on the calculation of the kurtosis for the detection of RFI in microwave radiometry," *IEEE Trans. Geosci. Remote Sens.*, vol. 46, no. 10, pp. 3129–3136, Oct. 2008.

[7] B. Güner, J. T. Johnson, and N. Niamsuwan, "Time and frequency blanking for radio-frequency interference mitigation in microwave radiometry," *IEEE Trans. Geosci. Remote Sens.*, vol. 45, no. 11, pp. 3672–3679, Nov. 2007.

[8] S. Misra, P. N. Mohammed, B. Güner, C. S. Ruf, J. R. Piepmeier, and J. T. Johnson, "Microwave radiometer radio-frequency interference detection algorithms: A comparative study," *IEEE Trans. Geosci. Remote Sens.*, vol. 47, no. 11, pp. 3742–3754, Nov. 2009.

[9] R. D. De Roo and S. Misra, "Effectiveness of the sixth moment to eliminate a kurtosis blind spot in the detection of interference in a radiometer," in *Proc. IEEE IGARSS*, Boston, MA, Jul. 7–11, 2008, vol. 2, pp. II-331–II-334.

[10] J. Piepmeier and F. Pellerano, "Mitigation of terrestrial radar interference in L-band spaceborne microwave radiometers," in *Proc. IEEE IGARSS*, Denver, CO, Jul. 31–Aug., 4, 2006, pp. 2292–2296.

[11] R. D. De Roo, "A simplified calculation of the kurtosis for RFI detection," *IEEE Trans. Geosci. Remote Sens.*, vol. 47, no. 11, pp. 3755–3760, Nov. 2009.

[12] M. G. Kendall and A. Stuart, *The Advanced Theory of Statistics*., 2nd ed. New York: Hafner, 1963.

[13] R. C. Geary, "A general expression for the moments of certain symmetrical functions of normal samples," *Biometrika*, vol. 25, no. 1/2, pp. 184–186, May 1933.

[14] I. S. Gradshteyn and I. M. Ryzhik, *Table of Integrals, Series, and Products*., 4th ed. New York: Academic, 1980.

[15] E. P. Adams and C. R. L. Hippisley, *Smithsonian Mathematical Formulae and Tables of Elliptic Functions*. Washington, DC: Smithsonian Inst., 1922, ser. Smithsonian Miscellaneous Collections.